



ELSEVIER

available at [www.sciencedirect.com](http://www.sciencedirect.com)journal homepage: <http://www.rpor.eu/>

## Therapeutic potential of atmospheric neutrons

Cyril Voyant<sup>a,b,\*</sup>, Rudy Roustit<sup>b</sup>, Jennifer Tatje<sup>b</sup>, Katia Biffi<sup>b</sup>, Delphine Leschi<sup>b</sup>, Jérôme Briañon<sup>b</sup>, Céline Lantieri Marcovici<sup>b</sup>

<sup>a</sup> University of Corsica, CNRS UMR SPE 6134, Campus Grimaldi, 20250 Corte, France

<sup>b</sup> Castelluccio Hospital, Radiotherapy Unit, BP 85, 20177 Ajaccio, France

### ARTICLE INFO

#### Article history:

Received 29 June 2010

Received in revised form

5 October 2010

Accepted 3 November 2010

#### Keywords:

NBCT

Neutron

Boron

Atmospheric

Glioblastoma

### ABSTRACT

**Background:** Glioblastoma multiform (GBM) is the most common and most aggressive type of primary brain tumour in humans. It has a very poor prognosis despite multi-modality treatments consisting of open craniotomy with surgical resection, followed by chemotherapy and/or radiotherapy. Recently, a new treatment has been proposed – Boron Neutron Capture Therapy (BNCT) – which exploits the interaction between Boron-10 atoms (introduced by vector molecules) and low energy neutrons produced by giant accelerators or nuclear reactors.

**Methods:** The objective of the present study is to compute the deposited dose using a natural source of neutrons (atmospheric neutrons). For this purpose, Monte Carlo computer simulations were carried out to estimate the dosimetric effects of a natural source of neutrons in the matter, to establish if atmospheric neutrons interact with vector molecules containing Boron-10.

**Results:** The doses produced (an average of 1  $\mu$ Gy in a 1g tumour) are not sufficient for therapeutic treatment of *in situ* tumours. However, the non-localised yet specific dosimetric properties of 10B vector molecules could prove interesting for the treatment of micro-metastases or as (neo)adjuvant treatment. On a cellular scale, the deposited dose is approximately 0.5 Gy/neutron impact.

**Conclusion:** It has been shown that BNCT may be used with a natural source of neutrons, and may potentially be useful for the treatment of micro-metastases. The atmospheric neutron flux is much lower than that utilized during standard NBCT. However the purpose of the proposed study is not to replace the ordinary NBCT but to test if naturally occurring atmospheric neutrons, considered to be an ionizing pollution at the Earth's surface, can be used in the treatment of a disease such as cancer. To finalize this study, it is necessary to quantify the biological effects of the physically deposited dose, taking into account the characteristics of the incident particles (alpha particle and Lithium atom) and radio-induced effects (by-stander and low dose effect). One of the aims of the presented paper is to propose to experimental teams (which would be interested in studying the phenomena) a simple way to calculate the dose deposition (allometric fit of free path, transmission factor of brain).

© 2010 Greater Poland Cancer Centre, Poland. Published by Elsevier Urban & Partner Sp. z.o.o. All rights reserved.

\* Corresponding author at: Castelluccio Hospital, Radiotherapy Unit, BP 85, 20177 Ajaccio, France. Tel.: +33 0495293666; fax: +33 0495293797. E-mail addresses: [cyrilvoyant@hotmail.com](mailto:cyrilvoyant@hotmail.com), [cyrilvoyant@gmail.com](mailto:cyrilvoyant@gmail.com) (C. Voyant).

### Nomenclature

$D_{ij}$	dose deposited by the reaction $i$ and the nucleus $j$ (Gy)
$N_0$	total number of neutron (NU)
$E$	energy variable (J)
$t$	time variable (s)
$S$	surface variable (m)
$N_j$	number of nuclei $j$ (NU)
$V$	volume ( $\text{m}^3$ )
$\sigma_{i\varphi}$	cross section for reaction $i$ and nucleus $j$ ( $\text{m}^2$ )
$E_{ij}^n$	energy deposited after the reaction $i$ on the nucleus $j$ (J)
$x$	depth (m)
$m$	mass (kg)
$\psi$	differential neutron flux ( $\text{J}^{-1} \text{s}^{-1} \text{m}^{-2}$ )
$\rho$	density ( $\text{g cm}^{-3}$ )
$\mu_{en}/\rho$	attenuation coefficient ( $\text{J kg}^{-1}$ )
$E_{a,s,b}$	neutron energy in air, skull and brain (J)
$L_{s,b,t}$	mean free path (m)
$T_{s,b,t}$	transmission factor for skull, brain and tumour (NU)
Depth	tumour depth in brain (m)
$F(E)$	cumulative distribution function for neutron related to energy (NU)
$n_i$	number of neutron with energy $i$ (NU)
$N_a$	Avogadro constant ( $\text{mol}^{-1}$ )
$A_j$	atomic mass number for nucleus $j$ (atomic mass unit, u)
$\sigma(E,j)$	total cross section for the nucleus $j$ and the energy $E$ ( $\text{m}^2$ )
$P_{E,j}$	capture probability on nucleus $j$ with the energy $E$ (NU)
$m_{rec}$	mass of recoil nucleus during elastic collision (kg)
$m_n$	neutron mass = 1.0087 u
$\varphi_{rec}$	deflexion angle in the system of the center of mass (rad)
$E_0$	energy of incident particle (J)
$w_r(E)$	weighting factor designed to reflect the different radiosensitivity of the tissues (NU)
$E_{i,f}$	initial and final neutron energy (J)

## 1. Background

In 2007, cancer caused about 13% of all human deaths (7.6 million). Some of the most invasive malignant tumours are breast cancer, colorectal cancer, lung cancer, and stomach and liver cancer. Brain tumours are not very common as they account for only 1.4% of all cancers in the United States. Patients with benign gliomas may survive for many years, but in most cases of glioblastoma multiforme (GBM), survival is limited to a few months after diagnosis without treatment.<sup>1,2</sup> Despite being the most prevalent form of primary brain tumour, GBM occurs in only 2–3 cases per 100,000 people in Europe and North America. It is the most common and most aggressive type of primary brain tumour in humans. The usual multimodality

treatment consists of open craniotomy with surgical resection of as much of the tumour as possible, followed by concurrent or sequential chemotherapy, antiangiogenic therapy with bevacizumab, gamma knife radiosurgery, standard radiotherapy, and symptomatic care with corticosteroids. Another therapeutic approach is based on the Boron Neutron Capture Therapy (BNCT) which was proposed in 1936 by Dr. Gordon Lecher only 4 years after the discovery of the neutron.<sup>3–5</sup> This method, which is well adapted for intra-cranial cancer treatments, is simple and well-designed in concept but complex and difficult in execution. It is based on the capacity of thermal neutrons to induce a reaction with Boron-10 nuclei, forming a compound nucleus (excited Boron-11 in Eqs. (1) and (2)) which then promptly disintegrates to Lithium-7 and an alpha particle (Fig. 1).<sup>6–8</sup> Both the alpha particle and the Lithium ion produce closely spaced ionizations in the immediate vicinity of the reaction, with a range of approximately 4 and 8  $\mu\text{m}$ , for Lithium-7 and alpha particle respectively, or roughly the diameter of one cell (10  $\mu\text{m}$ ).



This technique is advantageous since the radiation damage occurs over a short range and thus normal tissues can be spared. The path of the reaction products is shown in Fig. 2.

The NBCT is a well recognized treatment for GBM, particularly due to its efficiency, but is unfortunately very difficult to access as only a few radiotherapy units can use a proton accelerator.<sup>9,2</sup> In France, this service is not available to patients.

An alternative to this would be to find a new source of neutrons that is easily exploitable. Because free neutrons are unstable (mean lifetime of about 15 min), they can only be obtained from nuclear disintegrations, nuclear reactions, or high-energy reactions such as in cosmic radiation showers or collision accelerators. Cosmic radiation interacting with the Earth's atmosphere continuously generates neutrons.<sup>10–15</sup> The cosmic rays (essentially 85% of Hydrogen and 12.5% of Helium) penetrate the magnetic fields of the solar system and the Earth, and as they reach the Earth's atmosphere, they collide with atomic nuclei in the air (78% Nitrogen, 21% Oxygen and 1% Argon) to create cascades of secondary radiation of every kind. The intensity and energy distribution of different particles that make up atmospheric cosmic radiation vary in 3 essential parameters: altitude, location in the geomagnetic field (correlated to latitude, it deflects low-momentum charged particles back into space), and time in the sun's magnetic activity cycle.<sup>16–18</sup> Table 1 shows the implication of the first two (altitude and latitude). Atmospheric shielding, correlated to altitude, is determined by the thickness of the air mass above, called atmospheric depth.

At high altitude, geomagnetic latitude has a small effect on the shape of the neutron spectrum and a very large effect on the neutron radiative flux. In Fig. 3, representing the results found by Roesler in 1998,<sup>19</sup> we can see how strong an influence atmospheric depth has on the neutron flux. It decreases by a factor of 100 between high altitude (20 km corresponding to an atmospheric depth of 50  $\text{g cm}^{-2}$ ) and sea level (corresponding

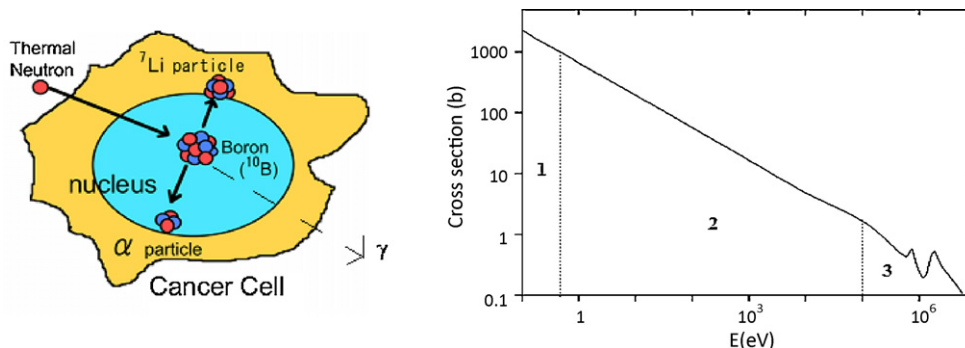


Fig. 1 – Schematic of  $^{10}\text{B}(n,\alpha)^7\text{Li}$  capture reaction in a cancer cell (left), and total cross-section (right) versus energy ((n,α0) and (n,α1)). Region 1 called low energy with mean cross section = 2000b; Region 2 middle energy with mean cross section = 20b; Region 3 high energy with mean cross section = 1b.

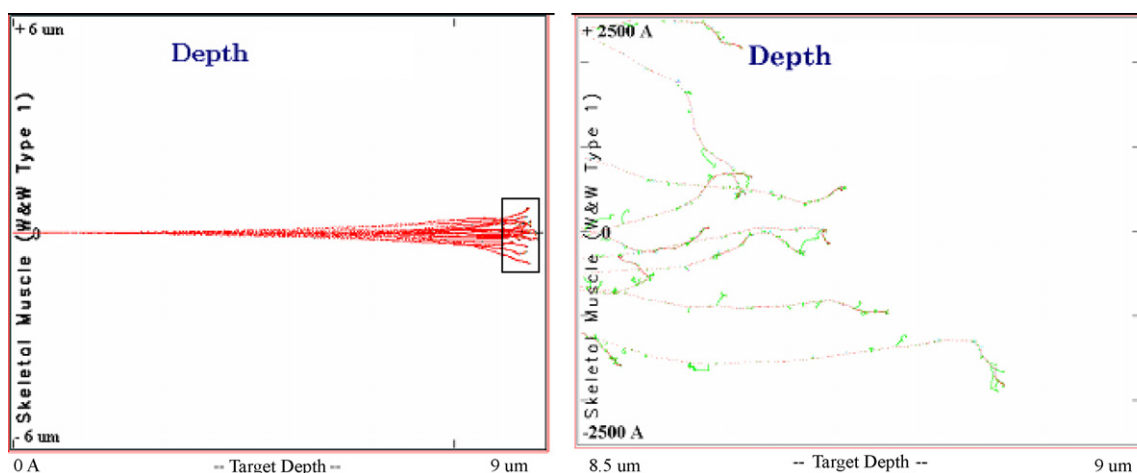


Fig. 2 – Penetration depth of alpha particle (1.47 MeV) in the muscle at left. On the right, the zoom of the last micrometer. Red points are the elastic scattering on hydrogenous nucleus, and green points the scattering of the secondary hydrogenous particle (SRIM® calculator). (For interpretation of the references to colour in this figure legend, the reader is referred to the web version of the article.)

to an atmospheric depth of  $1000 \text{ g cm}^{-2}$ ). Latitude is important as there is an increase by a factor of about 10 between the minimum intensity (at the Equator) and the maximum (at the Polar Regions).

The last parameter linked with the flux of atmospheric neutrons is solar variation. There are periodic components in these variations, mainly the 11-year solar cycle (or sunspot cycle), but also the solar magnetic activity cycle. It modulates the flux of high-energy galactic cosmic rays entering the solar system. As a consequence, the cosmic ray flux in the inner

solar system (or neutron flux in the atmosphere) is correlated with the overall level of solar activity.

## 2. Aim

The atmospheric neutron flux is much lower than that used during standard NBCT ( $10 \text{ n/s/cm}^2$  vs.  $10^9 \text{ n/s/cm}^2$ ). Small as this flux may be, its characteristics are certainly compatible for clinical use: free source for an ecological approach, frac-

Table 1 – Relation between neutron flux, altitude and geographic location.

Geographic location	Atmospheric depth ( $\text{g cm}^{-2}$ )	Altitude (km)	Neutron fluence rate ( $\text{cm}^{-2} \text{ s}^{-1}$ )
19°N, 127°W	53.5	20.3	1.24
54°N, 117°W	56	20.0	9.8
56°N, 121°W	101	16.2	9.6
38°N, 122°W	201	11.9	3.4
17°N, 76°W	1030	0	0.0127

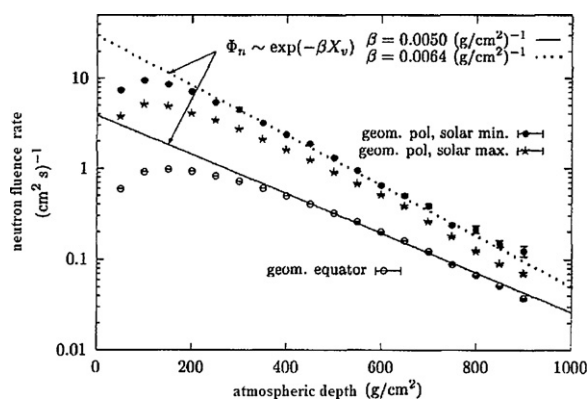


**Fig. 3 – The depth dependence of the neutron flux, calculations for three different conditions. Polar region (minimum and maximum) and equatorial region.**

tionated dose to allow normal cells to recover, localised dose deposition (only in tumour cells), and a disease being incurable (or hardly curable) with conventional tools. The purpose of the proposed study is not to replace the ordinary NBCT, but to test if naturally occurring atmospheric neutrons, considered to be an ionizing pollution at the Earth's surface, can be used in the treatment of a disease such as cancer. Before beginning the calculation, we know that atmospheric neutrons are not candidates to be considered for a global and single therapy (case of standard BNCT), however it is interesting to study the ability of atmospheric neutrons to be used as an adjuvant or neo-adjuvant treatment.

### 3. Materials and methods

#### 3.1. BSH ( $\text{Na}_2\text{B}_{12}\text{H}_{12}\text{S}_4$ ) and BPA( $\text{C}_9\text{H}_{12}\text{O}_4\text{BN}$ )

In clinical neutron capture therapy,  $^{10}\text{B}$  compounds such as BPA and BSH have been widely used as short-range alpha particle-producing agents.<sup>20–25</sup> It is believed that BSH, which has been clinically used in brain tumours, can pass through the disrupted blood–brain barrier and thus selectively accumulate in brain tumour tissue. BPA is an analogue of an essential amino acid phenylalanine, and is actively taken up in cells not only as an amino acid analogue for protein synthesis, but also as a tyrosine analogue for melanogenesis. Owing to this property, BPA has been clinically used for the treatment of malignant cells. To characterise these molecules, it is essential to quantify the nuclear reaction rate produced by the interaction with atmospheric neutrons. In this first study, we are not considering the concentration and the biological distribution of these molecules in the organism. We hypothesise that neutrons interact with carrier molecules and simulate the

different processes to establish which reactions are most probable. The estimation is done for all atmospheric neutrons (the full spectra are used). The cross sections were produced using ENDF/B library (available on <http://t2.lanl.gov>). Table 2 shows that the two molecules used in the simulation are appropriated for the neutron interaction: the alpha-producing reaction reveals to be the most frequent one (94% for BSH and 88% for BPA).

#### 3.2. Analytic dose expression

Before analytically calculating the absorbed dose into tissues<sup>1,26</sup> resulting from a succession of interactions between atmospheric neutrons and Boron nuclei, it is necessary to assume that the dose is comparable to kerma (transferred energy equals deposited energy) as the alpha and Lithium particles have a strong LET along with a very short pathway into the matter. Eqs. (3) and (4) stand for the expression of the average on-laid dose after a succession of interactions between neutrons and tissues. It becomes possible to define a mass coefficient of absorption denoted as  $(\mu_{en}/\rho)$  in Eq. (5).

$$d^3D_{ij} = \frac{d^3N_0}{dE dt dS} \frac{N_j}{V} \sigma_{ij} E_{ij}^n \frac{x}{m} dE dt dS \quad (3)$$

$$d^3D_{ij} = \psi \frac{N_j}{V^2} \sigma_{ij} E_{ij}^n \frac{x}{\rho} dE dt dS \quad (4)$$

$$d^3D_{ij} = \psi \left( \frac{\mu_{en}}{\rho} \right) dE dt dS \quad (5)$$

$E_{ij}^n$  is in fact equivalent to the Q-value of the reaction (default or excess of mass during the nuclear reaction). In the case of the radiative capture reaction, the value is nil as the dose will not be laid-on into the volume V. This method of calculation is relevant only in relatively simple cases. If we consider the lowering of the incident flux or a complex and heterogeneous substance, this method is impractical. Therefore, we have chosen to use a hybrid or mixed method which combines both an analytic model and Monte-Carlo type algorithms to quantify the doses in use.

#### 3.3. Modelling methodology

The characteristics of the matter (skull, brain and tumour) are essential to simulate the absorbed dose. We have chosen to use a detailed brain and skull composition as seen in Table 3. The tumour is considered similar to the brain (same chemical composition) with  $20 \mu\text{g/g}$  of Boron10 (average value found in the literature), representing 0.002% of a tumour weighing 1g.<sup>3</sup> The initial conditions are presented in Fig. 4. To simplify the calculation, only some reactions cross sections are chosen: (n,n), (n, $\alpha$ ) (n,p) and (n, $\gamma$ ).<sup>27</sup> This is a realistic hypothesis because other reactions are not frequent with the specific energy of atmospheric neutrons, their cross sections being too low. The simulation is done with the Visual-Basic programming language and the ENDF/B library. The computer used is a Xeon, 3GHz and 2GB (RAM). The ENDF/B evaluations are the basis for the nuclear data library used by radiation transport codes such as MCNP. The neutron flux spectrum used for the manipulation is measured at 12 km

**Table 2 – Nuclear reactions distribution after impact between neutron and BPA or BSH.**

	Radiative capture	(n, $\alpha$ )	(n,p)	(n,n)
BSH	1%	94%	~0%	5%
BPA	1%	88%	~0%	11%

**Table 3 – Brain and skull characteristics.**

Element	Isotope	Natural abundance (%)	Skull mass fraction (%) $\rho_s = 1.5 \text{ g/cm}^3$	Brain mass fraction (%) $\rho_b = 1.05 \text{ g/cm}^3$
H	1	99.985	3.4	9.5
	2	0.015		
C	12	100	15.52	18.5
	13	0.011		
O	16	99.862	43.54	65
	17	0.138		
N	14	99.634	4.2	3.5
	15	0.366		
Ca	40	96.941	22.51	1.5
	42	0.647		
	43	0.135		
	44	2.086		
	46	0.004		
	48	0.187		
P	31	100	10.31	1
S	32	95.02	0.3	0.2
	33	0.75		
	34	4.21		
	36	0.02		
Mg	24	78.93	0.21	0
	25	10		
	26	11.07		
K	39	93.26	0	0.4
	40	0.01		
	41	6.73		
Na	23	100	0	0.2
Cl	35	75.77	0	0.2
	37	24.23		

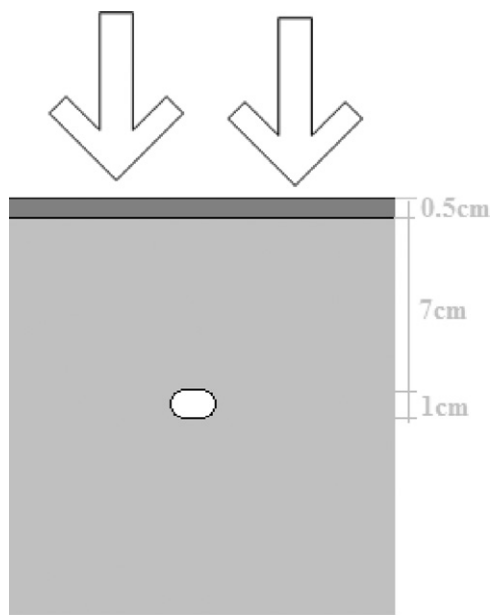


**Fig. 4 – Numerical phantom simulation.**

altitude and 45° latitude. The number of simulation events tested oscillates between 6000 and 60,000, but experiments show results are similar from 6000 simulations. The following

sections describe different steps of the simulation, as listed in Fig. 5.

**3.3.1. Cumulative distribution function related to neutron energy**

The first stage of the simulation determines the cumulative distribution of neutron energy in the air. This means calculating the function  $F = F(E)$ , described in Eq. (6), enabling to allocate a random number between 0 and 1 to a neutron incident energy. There are 14.7 neutrons/s/cm<sup>2</sup> in this particular case.

$$F(E) = \frac{\sum_{i=E_{\min}}^E n_i}{\sum_{i=E_{\min}}^{E_{\max}} n_i} \tag{6}$$

Once the incident energy has been allocated, the simulation requires estimating the interaction inside the brain and the skull. The tools used are the mean free paths and the transmission (attenuation) factors.

**3.3.2. Attenuation factor and neutron capture**

This parameter allows to quantify the number of neutrons (only capture type) interacting in the brain and the skull. The probability of neutron capture reactions is defined in Eq. (7), showing that the neutrons have merged to form a heavier

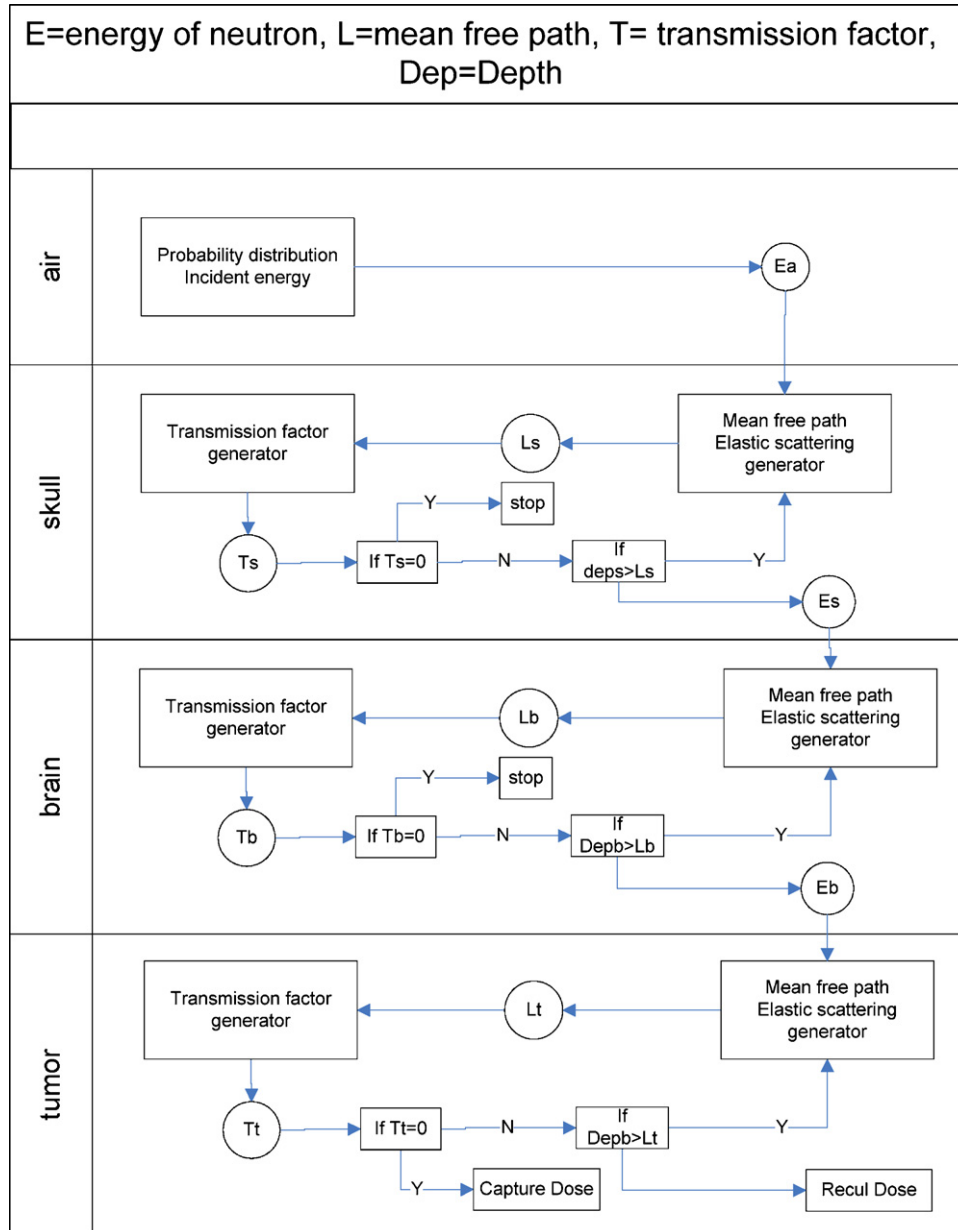


Fig. 5 – Schematic model used.

nucleus.

$$P_{E,j} = \rho \times N_a \frac{1}{A_j} \sigma(E, j) \tag{7}$$

The elastic and inelastic reactions (n,n) are not considered in the expression of the total capture cross sections because the neutrons continue to travel after impact. The transmission factor is calculated from the precedent probability factor by the expression  $T = 1 - \sum_j P_{E,j}$ . So, a coefficient of zero means the neutron is stopped in the matter and a coefficient of 1 means there is no capture at all. In the intermediate case, when the coefficient ranges between 0 and 1, a random number between 0 and 1 is compared to the transmission factor T. If this number is less than T, we consider there is no neutron

capture, otherwise the neutron is captured and stopped in the matter.

3.3.3. Mean free path

The mean free path of a particle is the average distance covered by the neutron between successive impacts. Alternatively, it is the distance at which the intensity of particles drops by 1/e. This coefficient is calculated with the following formula:

$$L = \sum_i \frac{A_i}{\rho N_a \sigma(E, i)} \tag{8}$$

In the case of mean free path for capture, the  $\sigma(E, i)$  is related to the reaction (n, $\alpha$ ) (n,p) and (n, $\gamma$ ), and for the elastic scattering

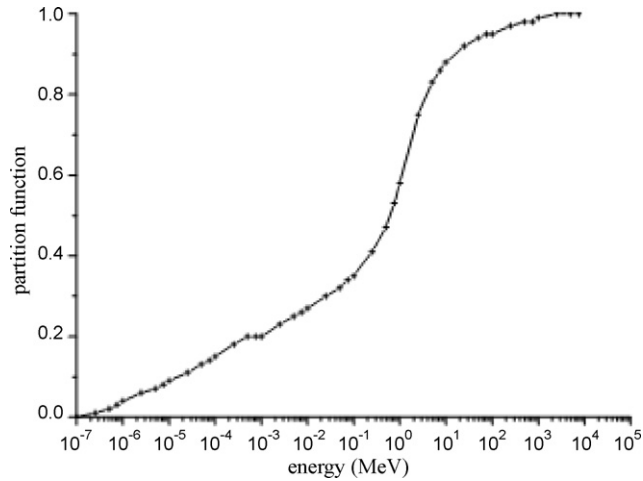


**Fig. 6 – Cumulative distribution function related to incident energy neutron.**

$\sigma(E, i)$ , it is only related to the elastic reaction.

3.3.4. Elastic interaction

We consider the energy loss is possible only with the elastic diffusion. All the capture reactions attenuate the beam but do not modify the energy of the incident particle. In the case of elastic collisions between neutrons and other particles, the energy lost is calculated in Eq. (9):

$$E_{rec} = E_0 \frac{4m_{rec}m_n}{(m_{rec} + m_n)^2} \cos^2 \varphi_{rec} \tag{9}$$

when  $E_0 < 10$  MeV, the reaction is isotropic and the cosine term is replaced by the factor 1/2. If the collision is done with a Hydrogen nucleus, the expression of the energy loss by the neutron is  $E_0/2$ .

**4. Results**

4.1. Air stage

The cumulative distribution function related to the incident neutron energy is represented in Fig. 6. This figure shows that the energy of atmospheric neutrons is very low. A random assortment from this function reveals that 50% of neutrons have energy of less than 1 MeV, and 80% of less than 10 MeV.

4.2. Skull stage

The thickness of the skull is about 0.5 cm, which generates a weak attenuation, as shown in Fig. 7. The transmission factor varies between 99.5% and 100%, meaning that very few neutrons are absorbed by the skull. The allometric fit of the results is described by  $T_s = 0.99997 - 0.00162E \text{ (eV)}^{-0.45609}$  ( $R^2 = 0.995$ ). This manipulation is done by the Origin Pro software. The second observation is related to the elastic interaction in the skull. The manipulation shows that the probability for a neutron to undergo an elastic interaction is less than 0.5%. In fact, the neutron flux is unchanged by crossing the skull.

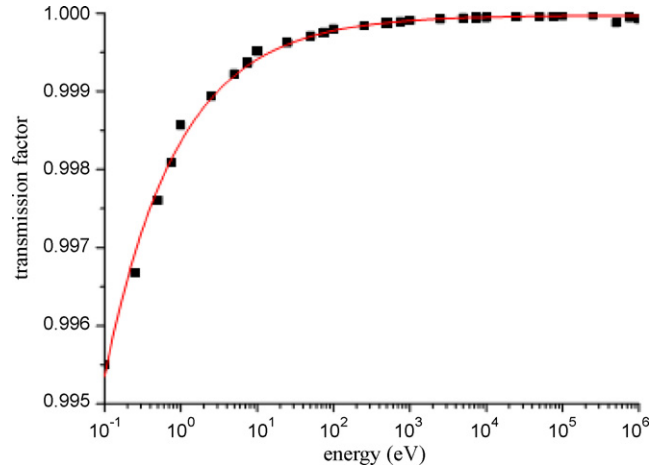


**Fig. 7 – Transmission factor for the skull (thickness 0.5 cm).**

**Table 4 – Mean free path in the brain, for the atmospheric neutrons. The average is related to the neutron energy distribution.**

Energy	L capture (cm)	L elastic (cm)
0.025 eV < ... < 0.5 eV	119	0.811
0.05 eV < ... < 1 keV	2360	0.815
1 keV < ... < 500 keV	32,600	1.54
500 keV < ... < 50 MeV	5460	8.58
0.025 eV < ... < 50 MeV	12,800	4.53

4.3. Brain stage

Without Boron (as in the healthy brain), neutrons have a higher probability of undergoing an elastic scattering process than a capture process. Table 4 shows the difference between those two modes. Capture reactions are rare, while those related to elastic collisions can be very frequent (every 1 cm for energies below 1 KeV). Neutrons with energies higher than 50MeV were not considered in this study because they are only in small amounts and more complex reactions begin to interfere. The allometric fit for the mean free path between two elastic collisions is given by  $L_b \text{ (cm)} = 0.81147 + 6.048 \cdot 10^{-5} E$

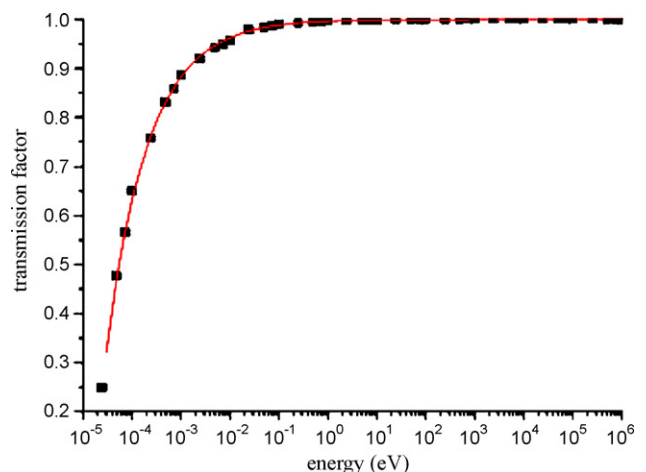


**Fig. 8 – Transmission factor for the brain.**

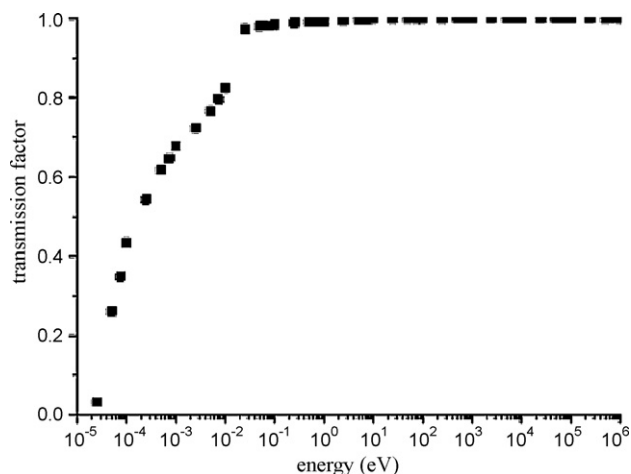


**Fig. 9 – Transmission factor for the tumour.**

(eV)<sup>0.78671</sup> ( $R^2=0.999$ ). The chosen method consists in determining whether, with this distance, the neutron will be captured or will continue on its path. If it is not mitigated, we consider it will lose some of its energy during the elastic collision. This method is repeated until the neutrons cross the brain and reaches the tumour. Fig. 8 shows the results for the transmission of neutrons during the passage through the brain. The analytic expression of this curve can be given by a standard allometric equation:  $T_s = 0.99943 - 0.003735E$  (eV)<sup>-0.49955</sup> ( $R^2=0.999$ ). We can observe that neutrons with energy higher than 0.1 eV will not be altered, and will continue on their path. During the simulations, we used the analytic expression of the transmission coefficients or the free average distance, which greatly reduce computation time (42 s instead of 15 h for 6000 neutrons).

#### 4.4. Tumour stage

As mentioned earlier, we consider that the tumour composition is equivalent to that of the brain comprising of Boron. The mean free paths of elastic collisions are almost equivalent to those shown in the previous section. However, the transmission factor will be changed. Collisions like (n,α) will be predominant at low energy, amending the first part of the transmission curve of the tumour (Fig. 9). The procedure is the same as that established in the case of the brain.

#### 4.5. Model validation

To validate the model and the method of calculation, we have made use of the SIEVERT calculation model (System of information and evaluation of flight exposure to cosmic radiation in transports, as available on [www.sievert-system.org](http://www.sievert-system.org)), a tool developed by IRSN. This tool allows quantifying the dose received by aircrew during a flight,<sup>28</sup> which is associated with the presence of neutrons at that altitude. Thus, we could compare the results given by our methodology with those established by the IRSN. In this manipulation, the numerical phantom does not contain Boron or tumour. We only simulated a flight and calculated the dose deposited in a cylindrical

model representing a person. The SIEVERT cuts airspace in 265,000 stitches according to altitude, latitude and longitude and then assigns them a dose rate (recalculated every month). For a flight from Paris to New York, the software simulates an effective dose of 6.1 μSv/h. We have made large approximations with the available data. The spectrum used corresponds to the one applied during the previous manipulation, for a similar latitude but at a different solar period. The simulation target is a cylinder 20 cm × 1.80 m with a weight of 56.5 kg. Its composition is the same as that previously described for the brain. As before, there are very few capture reactions. Furthermore, the only reactions of interest to us are the elastic reactions (n,n), the deposit dose caused by the recoil nucleus. The average energy transferred to the cylinder is calculated by  $\bar{D} = m^{-1} \sum (E_f - E_i) w_r(E)$ . The result of 4.37 μSv/h implies a difference of 30% with the reference SIEVERT. However, the numerous approximations make this result interesting and in accordance with the requirement we have set ourselves, namely to only work within the order of magnitude validating the interaction of atmospheric neutrons with the nuclei of Boron-10.

#### 4.6. Dosimetric aspect

The study of El Moussaoui et al.<sup>29</sup> shows that pre-filtering the neutron beam allows to ameliorate the registered depth dose, the incident energy of neutrons must be reduced to between 1 eV and 10 keV. To obtain this value, the Moroccan team simulated different “neutron decelerators” and noted the results. Inspired by this study, we studied the effects of a decelerator formed by water on the incidental spectra of neutrons. By interposing 10 cm (or 20 cm with less impact) of water between the beam and the test patient, we considerably increased the proportion of neutrons with energies ranging between 1 eV and 10 keV. The chosen simulation conditions are the attenuator of 10 cm of water, a crane thickness of 0.5 cm and a tumour of 1 cm containing 20 μg of Boron-10. The simulation is made with 6000 incident neutrons. In addition to changing the spectrum, the attenuator induced a neutron loss of 5% (capture reaction), but these are neutrons that would not have been able to reach the tumour because they mostly had a very low energy (Fig. 10). 5.6% of incident neutrons interact with the tumour, implying that the average dose to the tumour is in the order of 1 μGy for 1 h of irradiation (3000 interactions). We see that the value of the mean absorbed dose within the tumour is very low, so the use of this technique as a sole therapy at a tumour site seems inappropriate. However, given the irradiation heterogeneity and low runs of secondary particles (alpha and lithium), this dose does not present any “physical issue”, for better understanding we enter the field of micro dosimetry. The deposit is important but on a very small volume. Indeed, at the cell level represented by a cube of 1 μm<sup>3</sup>, where the dose will fill after a shock to the Boron-10, the absorbed dose is this time about 0.5 Gy/shock. Typically, this level of radiation induces important DNA base damage (i.e. for 1 Gy per cell, there are 2000 oxidised and reduced bases and 250 abasic sites, 1000 single and 40 double strand breaks, and 150 clustered lesions).<sup>30</sup> The non-localised, but specific, irradiation suggests this methodology as a possible source of treatment of micro-metastases (a form of metas-

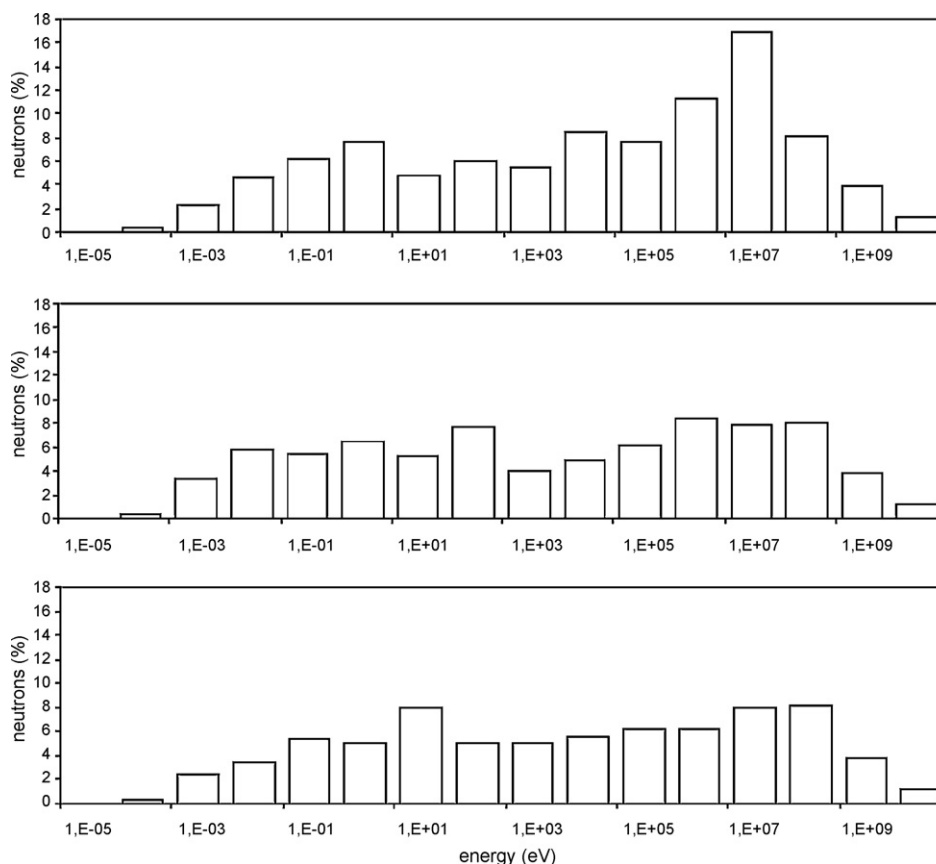


**Fig. 10 – Neutron spectra after interaction with attenuator (top, 5.12% of neutron stopped), brain (middle, 21.12% of neutron stopped) and tumour (bottom, 26.72% neutron stopped).**

tasis in which secondary tumours are too minuscule to be clinically detected). Adjuvant atmospheric NBCT would focus on destroying these micro-metastases. In addition, we must not forget that the exposure time and the concentration of Boron-10 (fixed at  $20\ \mu\text{g}$  for the study, but could be increased to at least  $50\ \mu\text{g}$ ) are directly proportional to the number of interactions. If one of these parameters increases, the number of interactions within the tumour will also increase. These values must also be contrasted with the different radiobiological effects inherent in the nature of secondary particles depositing dose (alpha and Lithium). A relatively weak dose rate, but with a well-targeted dose within a single cell, will lead to radiobiological effects. The first is related to the low dose rate effect,<sup>31</sup> the main effects of which are repair, repopulation and re-oxygenation which increase the radiosensitivity of the cells. This process is equivalent to the process observed during brachytherapy. The second aspect is related to the deleterious effects, such as mutagenesis, observed in cells that are not directly hit, a process called the by-stander effect.<sup>32,30</sup> Another effect to consider is where mutations are induced in cells that are hit only in the cytoplasm and not in the nucleus where DNA is located. Normal cells (without Boron) do not undergo a great dose deposition, at least no greater than during a standard flight. For these healthy cells, the ratio (concentration of boron) with malignant cells is about 10, revealing the low toxicity of Boron injection at altitude in healthy cells.

## 5. Conclusions

The present study shows that atmospheric neutrons can interact with Boron-10 found on molecular targets (BSH and BPA). These results were clearly predictable beforehand, but the code developed allows to quantify simply the dose after the penetration into the brain. However, the low flux of neutrons does not allow us to assume that it is possible to treat visible tumours (large cell colony), but rather micrometastases. To validate this hypothesis, the presented study must be completed with laboratory experiments to quantify the real effect of this radiation on the B-10 and biological cells. It is an intersection of several disciplines (microdosimetry, nuclear physics, bystander effect, low dose effect, etc.). The aim of the presented paper is to propose to experimental teams (which would be interested in studying the phenomena) a simple way to calculate the dose deposition (allometric fit of free path, transmission factor of brain). Moreover, the spectrum used as the basis for this study is a medium spectrum. Obviously, the flux will vary with location and altitude. Likewise, according to the injection protocol, the Boron concentration within GBM as well as the exposure duration will proportionally increase along with the on-laid dose. Sun cycle phases will equally modify the on-laid dose into the tumour. Considering the parameter values before maximising the atmospheric neutron output, we will be able to increase the absorbed dose

up to a hundred times. Although there are a lot of parameters which influence the dose rate, this radiation is not entirely uncontrollable. Previous calculation (not presented here) has shown that the use of dosimeter may allow to quantify the dose deposited in the tissue by neutron on Boron. The detectors studied (but all neutron detectors are certainly suitable) were luminescent materials (Optically Stimulated Luminescence) of a rare-earth-doped alkaline-earth sulfide with 2% of boron (SrS:Ce,Sm:B). The first results suggest that the dose in the tissue can be calculated by means of a dosimeter. In brief, further studies based on radio-induced effects occurring after the interaction between neutrons into GBM would make it possible to establish whether an aircraft may change into a radiotherapy room.

### Conflicts of interest

None.

### Acknowledgments

The authors thank Franglo-Traduction for their contributions during the drafting.

### REFERENCES

- Clark JC, Fronczek FR, Vicente HMG. Novel carboranylporphyrins for application in boron neutron capture therapy (BNCT) of tumors. *Tetrahedron Letters* 2005;46(14):2365–8.
- Laramore GE, Spence AM. Boron neutron capture therapy (BNCT) for high-grade gliomas of the brain: a cautionary note. *International Journal of Radiation Oncology, Biology, Physics* 1996;36(1):241–6.
- Dorn RV. Boron neutron capture therapy (BNCT): a radiation oncology perspective. *International Journal of Radiation Oncology, Biology, Physics* 1994;28(5):1189–201.
- Haritz D, Gabel D, Huiskamp R. Clinical phase-I study of Na<sub>2</sub>B<sub>12</sub>H<sub>11</sub>SH (BSH) in patients with malignant glioma as precondition for boron neutron capture therapy (BNCT). *International Journal of Radiation Oncology, Biology, Physics* 1994;28(5):1175–81.
- Yamamoto T, Matsumura A, Nakai K, Shibata Y, Endo K, Sakurai F, et al. Current clinical results of the Tsukuba BNCT trial. *Applied Radiation and Isotopes* 2004;61(5):1089–93.
- Hattori Y, Asano T, Niki Y, Kondoh H, Kirihata M, Yamaguchi Y, et al. Study on the compounds containing 19F and 10B atoms in a single molecule for the application to MRI and BNCT. *Bioorganic & Medicinal Chemistry* 2006;14(10):3258–62.
- Morand J, Moss R, Hachem S, Sauerwein W. A method to build an analytic model of the <sup>10</sup>B(n,α)<sup>7</sup>Li reaction rate space distribution for boron neutron capture therapy (BNCT). *Applied Radiation and Isotopes* 2009;67(7–8 (Suppl. 1)):S149–52.
- Nakagawa Y, Kageji T, Mizobuchi Y, Kumada H, Nakagawa Y. Clinical results of BNCT for malignant brain tumors in children. *Applied Radiation and Isotopes* 2009;67(7–8 (Suppl. 1)):S27–30.
- Kim K, Kim JK, Kim SY. Optimized therapeutic neutron beam for accelerator-based BNCT by analyzing the neutron angular distribution from <sup>7</sup>Li(p,n)<sup>7</sup>Be reaction. *Applied Radiation and Isotopes* 2009;67(7–8):1173–9.
- Boella G, Dilworth C, Panetti M, Scarsi L. The atmospheric and leakage flux of neutrons produced in the atmosphere by cosmic ray interactions. *Earth and Planetary Science Letters* 1968;4(5):393–8.
- Dudkin V, Potapov YU, Akopova A, Melkumyan L, Benton E, Frank A. Differential neutron energy spectra measured on spacecraft in low earth orbit. *International Journal of Radiation Applications and Instrumentation Part D Nuclear Tracks and Radiation Measurements* 1990;17(2):87–91.
- Goldhagen P, Clem JM, Wilson JW. Recent results from measurements of the energy spectrum of cosmic-ray induced neutrons aboard an ER-2 airplane and on the ground. *Advances in Space Research* 2003;32(1):35–40.
- Koi T, Muraki Y, Masuda K, Matsubara Y, Sako T, Murata T, et al. Attenuation of neutrons in the atmosphere and a thick carbon target. *Nuclear Instruments and Methods in Physics Research Section A: Accelerators, Spectrometers. Detectors and Associated Equipment* 2001;469(1):63–9.
- Kovaltsov GA, Usoskin IG. A new 3D numerical model of cosmogenic nuclide <sup>10</sup>Be production in the atmosphere. *Earth and Planetary Science Letters* 2010;291(1–4):182–8.
- Leray J. Effects of atmospheric neutrons on devices, at sea level and in avionics embedded systems. *Microelectronics Reliability* 2007;47(9–11):1827–35.
- Mavromichalaki H, Papaioannou A, Plainaki C, Sarlanis C, Souvatzoglou G, Gerontidou M, et al. Applications and usage of the real-time neutron monitor database. *Advances in Space Research*; doi:10.1016/j.asr.2010.02.019, in press.
- Phillips FM, Stone WD, Fabryka-Martin JT. An improved approach to calculating low-energy cosmic-ray neutron fluxes near the land/atmosphere interface. *Chemical Geology* 2001;175(3–4):689–701.
- Plainaki C, Mavromichalaki H, Belov A, Eroshenko E, Yanke V. Modeling the solar cosmic ray event of 13 December 2006 using ground level neutron monitor data. *Advances in Space Research* 2009;43(4):474–9.
- Roesler S, Heinrich W, Schraube H. Neutron spectra in the atmosphere from interactions of primary cosmic rays. *Advances in Space Research* 1998;21(12):1717–26.
- Ghaneolhosseini H, Tjarks W, Sjöberg S. Synthesis of novel boronated acridines- and spermidines as possible agents for BNCT. *Tetrahedron* 1998;54(15):3877–84.
- Gottumukkala V, Luguya R, Fronczek FR, Vicente MGH. Synthesis and cellular studies of an octa-anionic 5,10,15,20-tetra[3,5-(nido-carboranyl)methyl]phenyl]porphyrin (H<sub>2</sub>OCP) for application in BNCT. *Bioorganic & Medicinal Chemistry* 2005;13(5):1633–40.
- Heber E, Trivillin VA, Nigg D, Kreimann EL, Itoiz ME, Rebagliati RJ, et al. Biodistribution of GB-10 (Na<sub>210</sub>B<sub>10</sub>H<sub>10</sub>) compound for boron neutron capture therapy (BNCT) in an experimental model of oral cancer in the hamster cheek pouch. *Archives of Oral Biology* 2004;49(4):313–24.
- Jonnalagadda SC, Cruz JS, Connell RJ, Scott PM, Mereddy Venkatram R. Synthesis of [α]-carboranyl-[α]-acyloxy-amides as potential BNCT agents. *Tetrahedron Letters* 2009;50(30):4314–7.
- Lechtenberg B, Gabel D. Synthesis of a (B<sub>12</sub>H<sub>11</sub>S)<sub>2</sub>-containing glucuronoside as potential prodrug for BNCT. *Journal of Organometallic Chemistry* 2005;690(11):2780–2.
- Narayanasamy S, Thirumamagal BT, Johnsamuel J, Byun Y, Al-Madhoun AS, Usova E, et al. Hydrophilically enhanced 3-carboranyl thymidine analogues (3CTAs) for boron neutron capture therapy (BNCT) of cancer. *Bioorganic & Medicinal Chemistry* 2006;14(20):6886–99.
- Montgomery C, Montgomery D. The intensity of neutrons of thermal energy in the atmosphere at sea level. *Journal of the Franklin Institute* 1940;229(2):257–9.

27. Chin M, Spyrou N. A detailed Monte Carlo accounting of radiation transport in the brain during BNCT. *Applied Radiation and Isotopes* 2009;**67**(7-8 (Suppl. 1)):S164-7.
28. Vukovic B, Radolic V, Miklavcic I, Poje M, Varga M, Planinic J. Cosmic radiation dose in aircraft – a neutron track etch detector. *Journal of Environmental Radioactivity* 2007;**98**(3):264-73.
29. El Moussaoui F, El Bardouni T, Azahra M, Kamili A, Boukhal H. Monte Carlo calculation for the development of a BNCT neutron source (1 eV-10 KeV) using MCNP code. *Cancer/Radiotherapie* 2008;**12**(5):360-4.
30. Spothem-Maurizot M, Mostafavi M, Douki T, Belloni J. Radiation chemistry from basics to applications in material and life science. *EDP Science* 2008.
31. Hegyesi H, Benedek A, Kis E, Sáfrány G. Low dose radiation induced transcriptional alterations in directly irradiated and bystander fibroblast cells. *Radioprotection* 2008;**43**.
32. Mothersill C, Salbu B, Denbeigh J, Smith R, Heier L, Teien H, et al. Bystander effects induced by exposure to sublethal radiation and heavy metals in Atlantic Salmon. *Radioprotection* 2008;**43**.